Available online at www.sciencedirect.com
SCIENCE DIRECT®
Journal of Solid State Chemistry 177 (2004) 2323–2328
JOURNAL OF SOLID STATE CHEMISTRY
http://elsevier.com/locate/jssc

Raman scattering study and electrical properties characterization of elpasolite perovskites $Ln_2(BB')O_6$ (Ln = La, Sm…Gd and B, B' = Ni, Co, Mn)

Craig L. Bull[a,b,*] and Paul F. McMillan[a,b]

[a] *Davy-Faraday Research Laboratories, The Royal Institution of Great Britain, 21 Albemarle Street, London W1S 4BS, UK*
[b] *Department of Chemistry, UCL, Christopher Ingold Laboratories, 20 Gordon Street, London WC 1H 0AJ, UK*

Received 24 November 2003; received in revised form 8 February 2004; accepted 15 February 2004

Abstract

Two series of elpasolite perovskites Ln_2CoMnO_6 and Ln_2NiMnO_6 (Ln = La, Pr, Nd, Sm, Gd) have been prepared. The electronic band gap and magnetic Curie temperature vary systematically as a function of the rare earth cation size within both series. Here we used Raman scattering spectroscopy along with the results of previous structural studies to show that there is little change in octahedral distortion but significant changes in the octahedral tilting angle upon decreasing lanthanide ionic radius. The data indicate differences in the orbital overlap and bond strengths between the two series of materials that allow us to understand variations in the magnetic and electrical properties within and between the two perovskite series.

Keywords: Raman spectroscopy; Perovskites; Octahedral tilts; Electrical properties; Magnetism

1. Introduction

Transition metal-containing perovskites provide an important class of electronic and magnetic materials. The cubic perovskite aristotype (space group $Pm3m$) has general formula ABX_3, where the metal cations A and B are in 12-fold and octahedral coordination to the anion (X), respectively. This is the situation for $SrTiO_3$ at ambient pressure and temperature, and for $BaTiO_3$ above 120°C. Distortions from the ideal cubic structure can occur via by concerted rotations of the BO_6 octahedra, or by displacements of the A or B cations within their sites [1–3]. These distortions usually result in a lowered symmetry and an increased unit cell size. Such perovskite distortions are highly temperature- and pressure-dependent, and they can be tuned by changing the nature of the A and B cations, and they usually result in dramatic changes in the electronic properties. For example, distortion of the octahedral sites via off-center cation displacements relative to the O^{2-} sublattice results in the ferroelectric properties of titanate perovskites like $BaTiO_3$. Perovskite distortions can also affect the electronic band gap, and the magnetic properties.

Perovskites containing rare earth and transition metal cations on A and B sites exhibit interesting and useful electronic and magnetic properties. The A and B site substitutions can be adjusted to provide compounds with partial average oxidation states on the transition metal sublattice, resulting in materials with highly T-dependent magnetic and electronic behavior. The elpasolite perovskites Ln_2CoMnO_6 and Ln_2NiMnO_6 (Ln = La, Pr, Nd, Sm, Gd) studied here constitute two such series of compounds. In elpasolite perovskites, the basic formula unit is doubled by the presence of two B cations, i.e., $A_2BB'O_6$. However, the B site cations are often assumed to be disordered (i.e., $A(B_{0.5}B'_{0.5})O_3$), and the average unit cell size and symmetry of the aristotype are unaffected. However, ordering among the B site cations causes lowering of the perovskite symmetry, in addition to distortion of the metal sites, and tilting of the octahedra. Because of the similarity in scattering factors, it is not possible to determine ordering patterns among the transition metal B cations using X-ray powder diffraction. The elpasolite materials investigated

*Corresponding author. Fax: +20-76293569.
E-mail address: craig@ri.ac.uk (C.L. Bull).

0022-4596/$ - see front matter © 2004 Elsevier Inc. All rights reserved.
doi:10.1016/j.jssc.2004.02.022

here all possessed the same orthorhombic structure when studied using X-ray diffraction *Pnma* (D_{2h}^{16}, with $Z = 4$ $LnB_{0.5}B'_{0.5}O_3$ units) [4]. This is the same structure as the orthorhombic $GdFeO_3$ type compound, derived from the cubic aristotype by octahedral tilting. The tilting occurs in order to optimize the *Ln*–O bond distances by lowering the coordination number around the *A* site cation. The degree of tilt is expressed by the tolerance factor $t = d(A\text{–O})/\sqrt{2}d(\text{B–O})$, where d denotes interatomic distances calculated as the sum of the ionic radii of O^{2-} and *A* or *B* cations [5]. A tolerance factor which is equal or close to unity would be observed for perovskites with no tilt away from the ideal cubic structure (*Fm*3*m*).

In previous work, we used neutron scattering to investigate *B* site ordering within the elpasolite perovskite series. The results indicated significant ordering among *B* site cations, that permitted rationalization of the fact that resistivities of 50:50 Co:Mn and Ni:Mn materials were considerably larger than predicted from a random mixing model [4]. The effect of the ordering reduced the symmetry obtained from neutron diffraction analysis to monoclinic, space group $P2_1/n$. The neutron and X-ray diffraction studies were complemented by X-ray absorption spectroscopy and EXAFS studies of the local coordination around the transition metal cations. However, it was not possible to study the whole elpasolite series by that technique; due to overlap between *L* edges of some lanthanide ions and the EXAFS region just beyond the *K* edge for the transition metal ions. From the ensemble of structural results, however, it appears that *B*–O bond distances remained constant within both series presented in this study, and that only the octahedral tilt angle changes with decreasing lanthanide ionic radius, expressed in terms of the tolerance factor. This is correlated with systematic changes observed in the electronic and magnetic properties which has been studied extensively for the lanthanide based materials (La_2NiMnO_6 and La_2CoMnO_6) [6,7]. There is a systematic decrease in the magnetic ordering Curie temperature, indicating a decrease in orbital overlap within the TM–O sublattice, as a function of decreasing lanthanide ionic radius [8]. We have already demonstrated that the transition metal (TM) oxidation states in these materials are non-integral [9]. Systematic changes in the band gap with lanthanide cation radius are demonstrated here.

In the present study, we investigated the elpasolite series of $Ln_2BB'O_6$ perovskites by Raman scattering spectroscopy. Raman spectra has been performed extensively on perovskite systems and a large amount of useful information can be obtained from this technique [10,11]. The spectra provide additional information on octahedral tilting and distortion, that is complementary to the X-ray and neutron diffraction and EXAFS results. We use previously published data to assign vibrational modes within our spectra. The ensemble of the structural data allow variations in the electronic and magnetic properties to be correlated with the degree of octahedral tilting expressed in terms of the tolerance factor, as a function of the lanthanide cation radius.

2. Experimental

Monophasic, crystalline samples of Ln_2CoMnO_6 and Ln_2NiMnO_6 (where *Ln* = La, Pr, Nd, $Nd_{0.5}Sm_{0.5}$,[1] Sm, Eu and Gd) were prepared by a modified nitrate decomposition route. The synthesis has been described elsewhere [4]. Powder X-ray diffraction patterns were obtained using a Siemens D-500 diffractometer using Cu*K*α radiation.

Four-probe electrical resistivity measurements were obtained using pressed sintered discs. Electrodes were painted on to the samples using silver loaded paint and wires attached. The sample was then loaded into a modified Oxford Instruments cryostat and the sample cooled to 77 K. The electrical resistivity was then obtained at 10 K intervals to 300 K using a Fluke 8840A Multimeter. The band gap was calculated from an Arrhenius plot of resistivity vs. inverse temperature. SQUID magnetometry measurements were performed in order to obtain the magnetic ordering temperature of each sample. The measurements were carried out in a Quantum Design MPMS Squid at 1000 G (field cooled) between 5 and 300 K.

Raman spectra were obtained using a custom-built confocal micro-Raman system [12]. The incident laser (35 mW HeNe; $\lambda = 632.8$ nm) was focussed onto the sample using a Mitutoyo 50SL objective. Only a few mW of laser power were used as the samples tended to heat under the laser. The signal was collected in a backscattered geometry through the same objective. Two Kaiser® SuperNotch® filters discriminated the laser line from the Raman signal. The signal was collected using a Acton 500i spectrometer with a 500 mm focal length and a 1200 g/mm grating combined with a Princeton Instruments Spec-10-100B liquid nitrogen cooled back-illuminated silicon CCD.

3. Results and discussion

3.1. Structural studies

Powder X-ray diffraction patterns confirmed the materials to be monophasic. All patterns could be fully

[1] Because promethium is radioactive, it could not be used in the study. To simulate the effective ionic radius of Pm, a 50:50 mixture of Nd and Sm was used.

indexed in terms of an orthorhombic unit cell (*Pnma*, with $Z = 4$). The neutron diffraction data in fact indicated a reduction in symmetry to the monoclinic sub-group $P2_1/n$, due to *B* cation ordering. In the analysis of the vibrational spectra discussed below, we assumed an average *Pnma* symmetry to predict the Raman active modes in a first approximation, with the knowledge that the true local symmetry is lower than this.

The lattice parameters and unit cell volumes of members of the elpasolite perovskites studied are plotted as a function of lanthanide ionic radius in Fig. 1, and values are given in Table 1. There is a systematic decrease in unit cell volume with decreasing size of lanthanide ion for both series of materials, as expected. Among individual unit cell parameters, only a and b parameters decrease, and the **c**-axis parameter lengthens with decreasing lanthanide ion radius. This is consistent with an orthorhombic perovskite distortion caused by octahedral tilting, and it occurs in order to accommodate the displaced oxygen ion between the octahedra due to tilting, along the *c*-axis. The tolerance factor decreases systematically with decreasing lanthanide ionic radii (Table 1), and this parameter is correlated with the electronic and magnetic properties.

The average TM–O distances obtained from X-ray powder diffraction data were 1.94 Å for Co/Mn–O and 1.95 Å for Ni/Mn–O. Using neutron powder diffraction, individual octahedral bond lengths were established for Co- and Ni-centered polyhedra. The determined bond distances were: Co–O 1.99 Å, Ni–O = 2.01 Å, and Mn–O ≈ 1.89 Å, in agreement with EXAFS results [4,9].

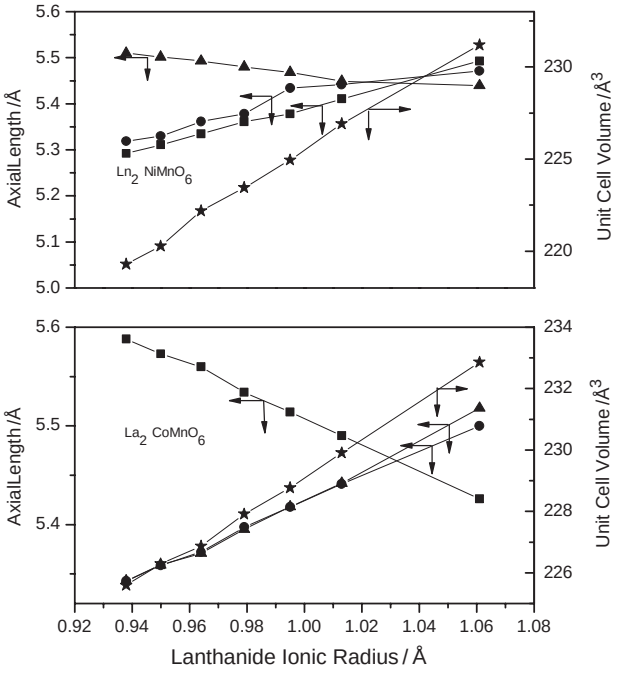

Fig. 1. Unit Cell parameters for the two series of materials Ln_2NiMnO_6 and Ln_2CoMnO_6 (★, unit cell volume; ▲, *a* axial length; ●, $b/\sqrt{2}$ axial length; ■, *c* axial length).

3.2. Raman spectra

The cubic perovskite aristotype has no Raman active vibrational modes. Distortions from cubic symmetry occur via co-operative rotation/tilting of octahedra, displacements of the *A* or *B* cations, or *B* site ordering. These result in an increased unit cell and reduction in the symmetry, so that Raman active modes appear at the Brillouin zone center. The number and relative intensity of peaks appearing in the Raman spectra is intimately related to the degree of distortion from the ideal cubic crystal structure. The Raman-active modes for a *Pnma* cell (assuming a disordered average elpasolite structure) are $7A_g + 7B_{1g} + 5B_{2g} + 5B_{3g}$. These can be classified as two symmetric and four asymmetric octahedral stretching modes, four bending modes, and six rotations or tilt modes of the octahedra. The other eight vibrations are associated with the lanthanide cations.

Raman spectra for the rare earth elpasolite perovskites studied here are shown in Fig. 2. The spectra are dominated by peaks at around 650 and 500 cm^{-1} that are readily assigned to octahedral *B*–O stretching vibrations. It is often useful to compare vibrations of solid-state materials with analogous fluoride or aquo complexes, whose vibrational spectra have been determined and assigned in the gas phase or for solution-phase complexes [13,14]. The spectra of the octahedral fluoride complexes $[MnF_6]^{2-}$, $[NiF_6]^{2-}$ and $[Co(H_2O)_6]^{2+}$ are summarized in Table 2. From this comparison, we can attribute to our assignment of the bands at 650 and 500 cm^{-1} as being associated with octahedral stretching vibrations.

The *B*–O stretching peaks of the elpasolite perovskites are broad and asymmetric. There are several reasons for this. First, the *B* and *B*′ sites are not completely ordered, and the different *B*–O stretching vibrations lie close in frequency, so that unresolved contributions from different BO_6 and $B'O_6$ environments are present within the band envelope. Second, the average (B, B') oxidation state is 3+. We have determined using X-ray absorption spectroscopy that in the Co, Mn series, the metal oxidation states are +2 and +4, respectively which are the more favorable oxidation states for the cobalt and manganese transition metal ions. However, in the Ni, Mn perovskites, the individual oxidation states are close to the average value, $+3 \pm \delta$ (where δ indicates a small shift away from the integer oxidation state) [9]. Because there is a dependence of *B*–O stretching frequency on the oxidation number of the metal cation, the band envelope also reflects a range in local oxidation state, depending upon the environment, that will then determine the covalency of the *B*–O bonding. Finally, ordering of B, B' cations results in a lowering of the

Table 1
Structural and physical properties of the two series of perovskites presented in this study

	a (Å)	b (Å)	c (Å)	t[a]	ρ (Ω cm)	E_g (eV)	T_c (K)
Ln (Ln_2CoMnO_6)							
La	5.426	7.778	5.518	0.879	350	0.75	233
Pr	5.49	7.695	5.442	0.864	1350	0.97	190
Nd	5.514	7.662	5.418	0.860	3300	1.15	175
$Nd_{0.5}Sm_{0.5}$	5.534	7.633	5.395	0.857	40,000	1.37	160
Sm	5.56	7.597	5.371	0.852	533,000	1.6	140
Eu	5.573	7.578	5.359	0.849	>106[b]	—	132
Gd	5.588	7.556	5.343	0.845	>106[b]	—	125
Ln (Ln_2NiMnO_6)							
La	5.439	7.737	5.493	0.871	541	0.9	287
Pr	5.449	7.696	5.411	0.856	619	1	255
Nd	5.468	7.685	5.378	0.853	659	1.02	222
$Nd_{0.5}Sm_{0.5}$	5.48	7.606	5.361	0.849	711	1.15	203
Sm	5.492	7.583	5.334	0.845	950	1.23	187
Eu	5.502	7.538	5.311	0.841	1282	1.32	159
Gd	5.510	7.522	5.292	0.838	1806	1.4	140

[a] The tolerance factor $t = d(A\text{–O})/2d(B\text{–O})$ see text for further description.
[b] The values of the resistivity were too high to be measured using our available equipment.

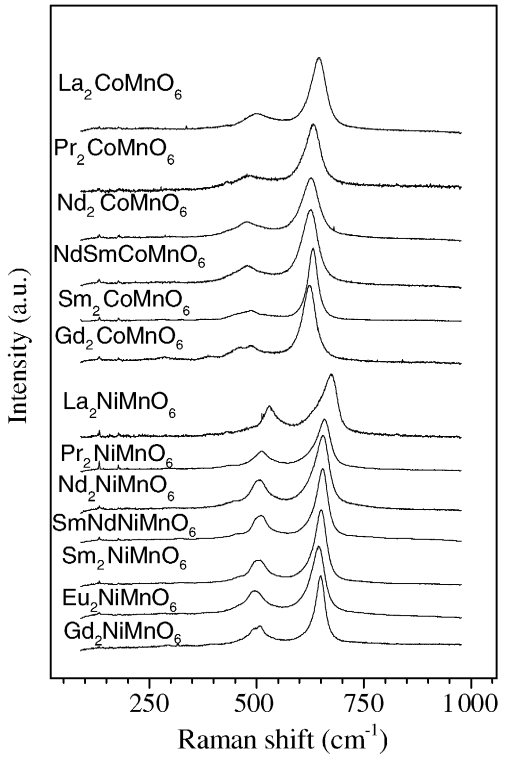

Fig. 2. Raman spectra of elpasolite perovskites studied.

symmetry, and thus a change in the Raman activity of *B*–O stretching vibrations. Domains with differing degrees of B, B' order will result in different contributions to the *B*–O stretching bands.

The *B*–O stretching bands for the Ni, Mn system lie approximately 30 cm^{-1} higher in energy than for the Co, Mn elpasolites. This is a surprising observation, because the average bond lengths in the two series are the same;

Table 2
Frequencies of MF_6 and $M^{2+}(H_2O)_6$ octahedra (all frequencies in cm^{-1}) [9].

	υ_1 (A_{1g})	υ_2 (E_g)	υ_3 (F_{1u})	υ_4 (F_{1u})	υ_5 (F_{2g})
$[MnF_6]^{2-}$	592	508	620	335	308
$[NiF_6]^{2-}$	562	520	658	345	310
[a]$[Co(H_2O)_6]^{2+}$	560	509	645		

[a] This work.

from the neutron studies, the Ni–O bonds are approximately 1% *longer* than the Co–O bonds. It has been shown previously that for $[VF6]^{n-}$ and other octahedral systems that with increasing *n* and hence decreasing oxidation state the energy of the vibrational modes decrease [13]. Other explanations include that, for the NiMn system, the TM–O and *Ln*–O bonds have a greater degree of covalency than within the CoMn system, due to an increased degree of orbital overlap in Ni, Mn elpasolites. This is consistent with measurements of the electrical and magnetic properties. It is also possible that the charge density of the transition metal can change the bond strength.

The octahedral *B*–O stretching peaks show only small variations in frequency within each series as a function of the lanthanide ionic radius (Fig. 3). This observation indicates that the changing size of the lanthanide cation is accommodated mainly by tilting/cooperative rotation of BO_6 octahedra, rather than deformation of the octahedra.

The low energy region of the elpasolite perovskite spectra shows several weak peaks, that are assigned to BO_6 tilting vibrations, that are coupled to *Ln*–O stretching (Fig. 4) [15]. The energy of each mode is plotted in Fig. 4 as a function of lanthanide ionic radius.

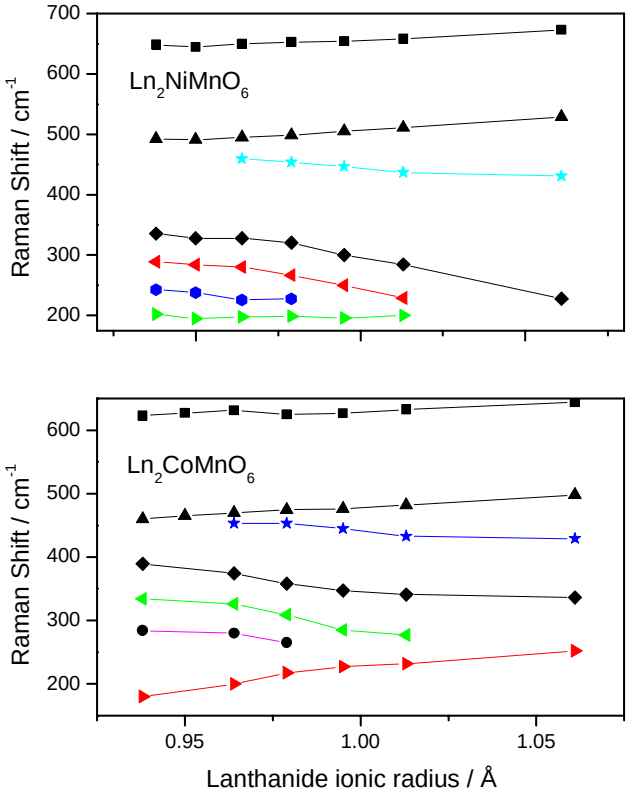

Fig. 3. Graph showing the variation in vibrational mode wavenumbers as a function of lanthanide ionic radius.

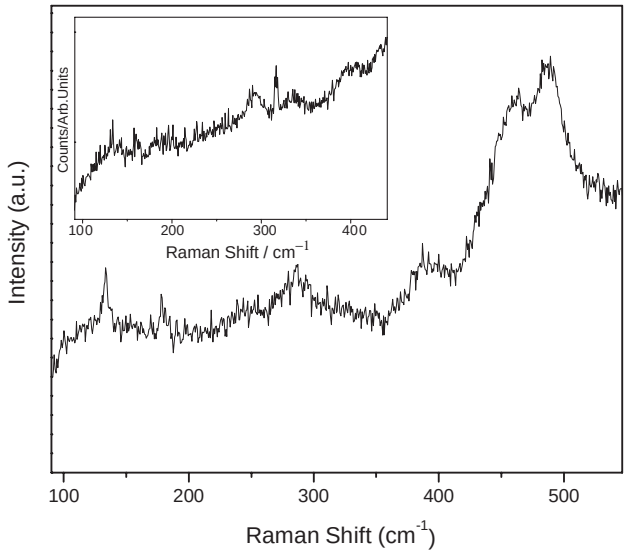

Fig. 4. Enlarged low energy region of Nd_2NiMnO_6 showing the weak vibrational modes due to octahedral tilting modes coupled to *Ln*–O vibrations. The inset shows the enlarged region of Gd_2NiMnO_6.

As expected, these vibrations are much more sensitive to changing lanthanide ionic radius. The peaks at 400, 325 and 275 cm^{-1} all decrease in energy with decreasing size of lanthanide ion. However, one mode increases in energy with decreasing size of lanthanide ion. This mode is associated with the B_{1g} tilt vibration and indicates that the degree of octahedral tilting is increasing with decreasing size of lanthanide ion. This tilting results in oxygen atoms being displaced in a specific direction, causing the *c*-axis to increase in length with decreasing lanthanide ionic radius.

The results of the Raman spectroscopic study are in agreement with the previous diffraction and XAS/EXAFS results [4,9], that the *B*–O octahedra remain approximately constant in dimension within each of the perovskite series, and that the decreasing lanthanide ionic radius is accommodated mainly by tilting of the octahedra around the large cation site, that is necessary in order to maintain the overall average bonding orbital overlap between the oxygen and lanthanide ions.

3.3. Electronic and magnetic properties

Systematic changes associated with the octahedral tilting angle and the lanthanide/transition metal cations can also be seen in the electronic and magnetic properties, which are controlled by orbital overlap of the TM–O–TM bond. One such property includes the magnetic Curie transition temperature. All materials studied were ferromagnetic: T_c for Ln_2NiMnO_6 is greater than that for Ln_2CoMnO_6 (Table 1) indicating a greater orbital overlap of the *B*–O–*B* bond between octahedra in the Ni, Mn series of materials compared with the Co, Mn elpasolites. A systematic relationship is observed between the ionic radius of the lanthanide ion and the Curie temperature (Fig. 5), that results from changes in the superexchange angle, in which the orbital overlap through which the exchange occurs decreases systematically with increasing lanthanide radius. Electron hopping occurs through the two interposed transition metal ions indirectly through an intervening oxygen

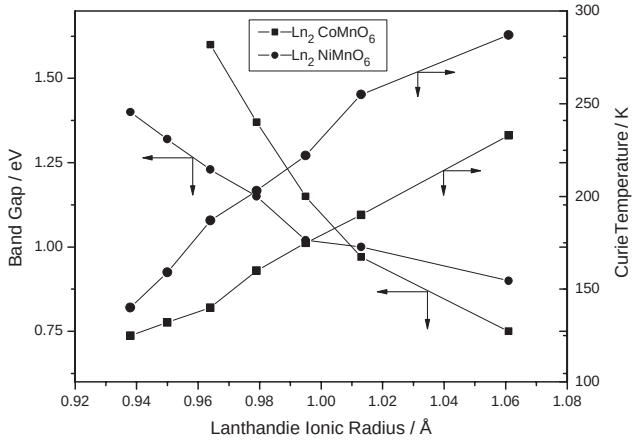

Fig. 5. Plot of electrical band gap and magnetic Curie temperature as a function of lanthanide ionic radius for Ln_2CoMnO_6 (■) and Ln_2NiMnO_6 (●).

atom. As the angle of exchange decreases from 180° to a smaller value, the extent of exchange also decreases. The superexchange angle or orbital overlap is thus determined by the *B*–O–*B*′ bond or octahedral tilt angle, that is lowered as the size of the lanthanide ion decreases. These structural changes are documented in the Raman spectra, suggested by the X-ray diffraction data and can be inferred by comparison of the tolerance factor.

The electrical resistivity and the associated band gap in semiconducting perovskites [16] are primarily governed by the *B*–O sublattice, through which the conduction and valence bands are formed via orbital overlaps along the distorted cube edges. The magnitude of the orbital overlap is determined by geometrical factors, i.e., the *B*–O–*B*′ bond angle, and the nature of the ions involved. With decreasing orbital overlap, there is an expected increase in resistivity and the band gap, as the conduction and valence band become further separated in energy. Therefore, with decreasing lanthanide ionic radius, and hence an increase in the octahedral tilt angle, the band gap and electrical resistivity both increase, as is observed within the elpasolite series studied here (Fig. 5; Table 1). During the experiment the result is checked to ensure that the behavior observed is due the ohmic nature of the material and hence the contacts are reversed and the measurement is taken at different values of current. We note that the electrical resistivity measurements have only been performed using pressed powders (at 10 tonne), and the values of the resistivities (and hence band gap) obtained can only be taken as an indication of the true resistivity (and band gap) as a single crystal is required for definitive electrical measurements. The pressing of powders may introduce voids, which will affect the resistivity and there may be inherent grain boundary effects that will alter the real value of the resistivity. The resistivity and band gap values may also be altered by the addition of other temperature dependent carrier production effects [17].

It has been suggested that, as the acidity of the lanthanide decreases (i.e., the tendency to withdraw electrons from its neighbors), the covalency of adjacent *B*–O bonds should increase [18,19]. As the covalency of the *B*–O bond decreases, the electrons become more localized, and they have a lowered tendency to conductivity *via* a hopping mechanism. The localization of electrons means that the bandwidth is lowered, contributing to the overall change in band gap and resistivity with changing lanthanide ionic radius. This is consistent with the observed behavior within in the samples studied here. Similar covalency effects have been describe changes in the related $Tl\mathit{Ln}X_2$ series where, as the *Ln*–*X* bond decreases in length, the lanthanide decreases in ionic radius and hence the covalency of the Tl–*X* bond increases, whereas the *Ln*–*X* bond covalency decreases (*X*=O or halide) [20].

4. Conclusions

We have shown by use of Raman spectroscopy that upon decreasing the lanthanide ionic radius in the series of materials Ln_2CoMnO_6 and Ln_2NiMnO_6 there is no significant change in the octahedral distortion within each series. However, there is a significant change in the octahedral tilting parameter across the series. The change in octahedral tilting angle occurs in order to maintain the total orbital overlap between the O^{2-} and Ln^{3+} (*Ln* = La, Pr, Nd, Sm, Gd) ions. The variation in *B*–O–*B*′ angles associated with the tilting is used to understand the changes in magnetic and electrical properties that occur as a result of decreasing orbital overlap within the BO_6 sublattice within the series.

Acknowledgments

CLB wishes to thank DERA for funding the synthesis of these samples. The help of Richard Mortimer is gratefully acknowledged. The remainder of the work was supported by a Wolfson Foundation Research Merit Award to PFM. The Raman spectroscopy system at UCL was constructed with funds from EPSRC. Emmanuel Soignard is gratefully acknowledged for assistance in obtaining the spectra.

References

[1] K.S. Knight, Solid State Ionics 145 (2001) 275.
[2] A.M. Glazer, Acta Crystallogr. B 28 (1972) 981.
[3] P.M. Woodward, Acta Crystallogr. B 53 (1997) 32.
[4] C.L. Bull, D. Gleeson, K.S. Knight, J. Phys.: Condens. Matter 15 (2003) 4927.
[5] N. Ramadass, Mater. Sci. Eng. 36 (1978) 231.
[6] R.I. Dass, J.B. Goodenough, Phys. Rev. B 67 (2003) 014401.
[7] R.I. Dass, J.B. Goodenough, Phys. Rev. B 68 (2003) 064415.
[8] J.B. Goodenough, A. Wold, R.J. Arnott, N. Manjuk, Phys. Rev. 24 (1961) 373.
[9] C.L. Bull, G. Sankar, D. Gleeson, C.R.A. Catlow, G.D. Price, in preparation.
[10] L. Martin-Carron, A. de Andres, M.J. Martinez-Lope, et al., Phys. Rev. B 66 (2002) 174303.
[11] M.N. Illiev, M.V. Abrashev, H.-G. Lee, et al., Phys. Rev. B 57 (5) (1998) 2872.
[12] E. Soignard, P.F. McMillan, in preparation.
[13] K. Nakamoto, Infrared and Raman Spectra of Inorganic and Coordination Compounds, 3rd Edition, Wiley-Interscience, New York, 1978.
[14] Q. Williams, R. Jeanloz, P. McMillan, J. Geophys. Res. 92 (1987) 8116.
[15] V.A. Amelitchev, B. Guttler, O.Yu. Gorbenko, A.R. Kaul, A.A. Bosak, A.Yu. Ganin, Phys. Rev. B 63 (2001) 104430.
[16] B.C. Tofield, W.R. Scott, J. Solid State Chem. 10 (1974) 183.
[17] C.G. Koops, Phys. Rev. 83 (1951) 121.
[18] J.B. Goodenough, Prog. Solid State Chem. 5 (1971) 149.
[19] P.M. Raccah, J.B. Goodenough, Phys. Rev. 155 (3) (1967) 932.
[20] M. Duczmal, L. Pawlak, J. Alloys Compds. 262–263 (1997) 316.